CHEMISTRY
A EUROPEAN JOURNAL

DOI: 10.1002/chem.201001038

# Platinum Nanoflowers on Scratched Silicon by Galvanic Displacement for an Effective SALDI Substrate**

Hideya Kawasaki,*[a] Teruyuki Yao,[a] Takashi Suganuma,[a] Kouji Okumura,[a] Yuichi Iwaki,[a] Tetsu Yonezawa,[b] Tatsuya Kikuchi,[b] and Ryuichi Arakawa*[a]

**Abstract:** We report a new and facile method for synthesizing 3D platinum nanoflowers (Pt Nfs) on a scratched silicon substrate by electroless galvanic displacement and discuss the applications of the Pt Nfs in surface-assisted laser desorption/ionization-mass spectrometry (SALDI-MS). Surface scratching of n-type silicon is essential to induce Pt Nf growth on a silicon substrate (to obtain a Pt Nf silicon hybrid plate) by the galvanic displacement reaction. The Pt Nf silicon hybrid plate showed excellent SALDI activity in terms of the efficient generation of protonated molecular ions in the absence of a citrate buffer. We propose that the acidity of the Si–OH moieties on silicon increases because of the electron-withdrawing nature of the Pt Nfs; hence, proton transfer from the Si–OH groups to the analyte molecules is enhanced, and finally, thermal desorption of the analyte ions from the surface occurs. Signal enhancement was observed for protonated molecular ions produced from a titania nanotube array (TNA) substrate on which Pt nanoparticles had been photochemically deposited. Moreover, surface modification of the Pt Nf silicon hybrid plate by perfluorodecyltrichlorosilane (FDTS) (to obtain an FDTS-Pt Nf silicon hybrid plate) was found to facilitate soft SALDI of labile compounds. More interestingly, the FDTS-Pt Nf silicon hybrid plate acts 1) as a high-affinity substrate for phosphopeptides and 2) as a SALDI substrate. The feasibility of using the FDTS-Pt Nf silicon hybrid plate for SALDI-MS has been demonstrated by using a β-casein digest and various analytes, including small molecules, peptides, phosphopeptides, phospholipids, carbohydrates, and synthetic polymers. The hybridization of Pt Nfs with a scratched silicon substrate has been found to be important for achieving excellent SALDI activity.

**Keywords:** galvanic displacement · hybrid materials · mass spectrometry · platinum · surface chemistry

## Introduction

Matrix-assisted laser desorption/ionization mass spectrometry (MALDI-MS) using organic matrices is a soft ionization technique that causes very little fragmentation of the analytes.[1,2] By using UV-absorbing organic acids, such as 2,5-dihydroxybenzoic acid (DHBA) and α-cyano-4-hydroxycinnamic acid (CHCA) in MALDI-MS, various compounds such as polymers, peptides, and lipids, as well as complex mixtures in high-salt matrices and buffers, can be analyzed.[3,4] However, matrix ion interference and detector saturation are inevitable in the MALDI-MS analysis of low-mass molecules ($m/z < 500$), and this makes the characterization of small molecules difficult despite the significance of such characterization. Various approaches involving the use of organic-matrix-free LDI-MS have been investigated for analyzing small molecules in a MALDI instrument.[5] Siuzdak and co-workers developed a matrix-free LDI-MS method for generating intact molecular ions by using porous silicon, which has high UV absorbance and a high surface

[a] Dr. H. Kawasaki, T. Yao, T. Suganuma, K. Okumura, Dr. Y. Iwaki, Prof. R. Arakawa
Department of Chemistry and Materials Engineering
Faculty of Chemistry, Materials and Bioengineering
Kansai University, 3-3-35 Yamate-cho, Suita-shi
Osaka, 564-8680 (Japan)
Fax: (+81) 6-6339-4026
E-mail: hkawa@kansai-u.ac.jp
arak@kansai-u.ac.jp

[b] Prof. T. Yonezawa, T. Kikuchi
Division of Materials Science and Engineering
Faculty of Engineering, Hokkaido University
Kita 13, Nishi 8, Kita-ku, Sapporo
Hokkaido 060-8628 (Japan)

[**] SALDI = surface-assisted laser desorption/ionization

Supporting information for this article is available on the WWW under http://dx.doi.org/10.1002/chem.201001038.

area.[6] This method is known as desorption ionization from porous silicon (DIOS). In contrast to MALDI, DIOS does not use organic matrices, and hence, one of its most important features is the absence of matrix interferences in the low-mass region. Therefore, in DIOS, the detectable mass range of small biomolecules, pharmaceutical compounds, amino acids, and oligopeptides can be extended to below $m/z$ 500.[7–9]

More recently, several other types of nanostructured substrates for organic-matrix-free LDI-MS have been reported. In particular, silicon-based nanomaterials, including nanostructured silicon films,[10] silicon nanowires,[11,12] silicon nanocavity arrays,[13,14] silicon microcolumn arrays,[15] and amorphous silicon,[16] have been extensively studied, and a new technique known as nanostructure-initiator mass spectrometry (NIMS) has recently been proposed.[17] Metal-oxide-based semiconductors with good UV absorbance are also promising candidates for matrix-free LDI-MS applications, such as titania sol–gel films,[18] titania nanotube arrays,[19] zinc oxide nanowires,[20] mesoporous tungsten titanium oxides,[21] and germanium nanodots.[22] In addition, double- or multilayer-coated hybrid substrates, such as metal-coated porous alumina (platinum/alumina),[23,24] two-layered amorphous silicon,[25] titania-printed aluminum foils (titania/aluminum),[26] silver-particle-deposited porous silicon (silver/silicon),[27] gold nanorods on porous alumina (gold/alumina),[28] layer-by-layer (LBL) self-assembled films (polymer/gold),[29,30] DVDs coated with diamond-like carbon,[31] cationic-polymer-coated graphite sheets (polymer/graphite),[32] and cobalt-coated silicon substrates (cobalt/silicon),[33] are considered as promising materials for matrix-free LDI-MS because the layer properties of these substances can be varied independently; further, these hybridization effects can improve the efficiency of matrix-free LDI-MS.

Another approach for the LDI-MS analysis of small molecules involves the use of nanoparticles as matrices, such as graphite,[34] carbon nanotubes (CNTs),[35] ZnO,[36] $TiO_2$,[37–39] $Fe_2O_3$,[40] $Fe_2O_3/TiO_2$,[41] Pt,[42] Au,[43–47] Ag,[48,49] FePtCu,[50] ZnS,[51] CsSe,[52] and $EuF_3$[53] nanoparticles. The use of nanoparticles with a high surface area is extremely advantageous for sample pretreatment, especially for the separation and enrichment of target molecules from mixtures in LDI-MS analysis. In this paper, "surface-assisted laser desorption/ionization" (SALDI) refers to both nanoparticle matrices and nanostructured substrates, although the meaning of the technical terms used in this field is somewhat unclear. There is no consensus on the mechanism underlying SALDI, but some factors that promote desorption/ionization efficiency have been reported: 1) laser-induced rapid temperature increase,[54] 2) substrates with a high surface area (porous, groove-like, nanowires, and nanodots),[54,55] 3) solvent molecules,[14,56] 4) surface functionalities such as terminal OH groups or a hydrophobic surface,[12,32,46,57–59] 5) electrically conductive surfaces,[23] and 6) laser-induced surface melting/restructuring.[60–62]

In our previous studies, we focused on SALDI-MS using various metal nanoparticles, such as Pt, Au, Ag, and Cu nanoparticles, for the analysis of peptides, and we observed that the SALDI performance was superior when Pt nanoparticles were used.[63] In addition, we developed a SALDI-MS method by using Pt nanoparticles with thin projections on the surface (termed Pt Nfs); in this case, the performance of the SALDI-MS for biomolecules, that is, the sensitivity to peptides and the efficiency of detecting proteins in the presence of a citrate buffer,[42] was further improved. However, these Pt nanomaterials and other nanomaterials have limited applications in SALDI-MS for the following reasons: 1) the efficiency of generating protonated molecular ions is low, and 2) the SALDI process, being "harder" than MALDI, causes fragmentation of labile compounds. Pt nanomaterials show sufficiently high UV absorbance, but are inefficient for producing protonated species in the absence of citrate buffer additives. The use of a citrate buffer as an effective proton source helps to obtain proton adducts, but molecular ion peaks from the citrate often appear in the low-mass region (below $m/z$ 500) in the spectrum; hence, this organic-matrix-free approach becomes less advantageous for SALDI-MS. Such an inefficiency in the generation of protonated species has also been reported in other SALDI-MS methods involving the use of Au,[29,43,46] $TiO_2$,[18] and CNTs.[64] Another disadvantage of SALDI is that it is relatively "hard" compared with MALDI. When using Pt nanomaterials, a very small peak corresponding to the intact molecular ion generated from 1,2-dimyristoyl-sn-glycero-3-phosphocholine (DMPC) is observed in the SALDI mass spectrum; this is because the spectrum includes significant peaks corresponding to the fragments ($m/z$ 184 and 86) from the polar head group.[42] In DIOS-MS as well, fragment ion peaks corresponding to DMPC are predominant in the spectrum, and the molecular ion peak is indistinct.[65] This hard ionization tendency has also been reported for SALDI-MS employing Au nanoparticles[63] or carbon-based materials.[32] Thus, achievement of a soft SALDI process with a low degree of fragmentation and the efficient generation of protonated molecular ions without the use of a citrate buffer additive remain unresolved issues in SALDI-MS.

To increase the efficiency of generating protonated molecular ions and to achieve a "soft" SALDI process, we propose a new and facile method that employs Pt nanoflowers (Pt Nfs). We first synthesized 3D Pt Nfs on a silicon substrate by electroless galvanic displacement and investigated the application of these Pt Nfs in SALDI-MS. Here, we define Pt nanoflowers as Pt nanoparticles with many nanometer-scale surface projections. The plate was simply prepared by immersing an n-type silicon substrate into an aqueous solution of HF containing a Pt salt, whereupon direct growth of Pt Nfs on the silicon surface proceeded spontaneously through an electroless galvanic reaction between the aqueous solution of Pt salt and the silicon substrate. Surface scratching of the n-type silicon proved to be essential for inducing Pt Nf growth on a silicon wafer (to obtain a Pt Nf silicon hybrid plate) by galvanic displacement. This method differs from the previously reported electroless galvanic displacement methods, which afforded spherical Pt particles on

  

the silicon surface.[66,67] The Pt Nf silicon hybrid plate showed excellent SALDI activity in terms of the efficient generation of protonated molecular ions in the absence of a citrate buffer. To achieve "soft" SALDI, the Pt Nf silicon hybrid plate was further modified with perfluorodecyltrichlorosilane (FDTS) via the surface OH groups on the silicon substrate (to obtain an FDTS-Pt Nf silicon hybrid plate). More interestingly, we found that, similar to $TiO_2$ substrates,[26,41] the FDTS-Pt Nf silicon hybrid plate acts as an efficient solid-extract plate and selectively absorbs phosphorylated peptides from a complex analytical mixture. The FDTS-Pt Nf silicon hybrid plate can act as an affinity substrate for phosphopeptides as well as a SALDI substrate.

## Results and Discussion

**Fabrication of Pt Nfs on scratched silicon surfaces by galvanic displacement and their characterization**: Galvanic deposition of Pt on silicon was carried out according to a local cell mechanism, which involves local cathode deposition of Pt particles by the injection of holes into the valence band of n-type silicon and local anode dissolution of silicon by the injected holes and HF.[66,67] Thus, the reduction of Pt ions and the chemical etching of silicon occur simultaneously at the silicon surface in the absence of an externally applied potential. Previously, galvanic deposition of Pt particles on a silicon wafer has been reported to afford spherical Pt particles;[68–70] these studies were focused on controlling the size and density of the Pt particles. By using a scratched silicon substrate in the present study, we induced the direct growth of 3D Pt Nfs with anisotropic shapes on a silicon wafer (to obtain a Pt Nf silicon hybrid plate) by galvanic displacement. The scratched silicon wafer was prepared by manual grinding of an n-type silicon wafer with sandpaper (#1000). Galvanic deposition of Pt on these scratched silicon substrates was performed by using an aqueous solution of 1 mM $H_2PtCl_6$ for various immersion times. After immersion times in excess of 10 min, SEM images of the Pt Nf silicon hybrid plate (Figure 1) revealed the formation of non-spherical structures with numerous thin irregular projections on their surfaces, similar to petals; these projections give rise to flower-like structures (Pt Nfs) on the scratched silicon plate. The size of the individual Pt Nfs was in the range 100–300 nm; these Pt Nfs further assembled to form large 3D aggregates that were a few microns in size. The Pt Nf silicon hybrid plate was obtained without the use of any capping molecule/surfactant. When the immersion time was 10 min, the Pt Nfs did not cover the silicon substrate completely, but tiny Pt Nfs formed around large Pt Nfs. When the immersion time was increased to 60 min (Figure 1c and d), the tiny Pt Nfs grew in size and assembled to form large 3D Pt Nfs. Interestingly, the projections on the surfaces of the Pt Nfs grew further, as shown in Figure 1d). In contrast, when we used an n-type silicon wafer without scratching, as in our previous paper,[68] spherical Pt particles were formed on the silicon surface. This difference clearly shows that the use of a scratched silicon wafer is essential for the formation of Pt Nfs. Although the detailed mechanism of the Pt Nf growth is not clear at present, it is apparent that surface scratching of the silicon wafer produces defect sites such as step edges, pits, and dangling bonds on its surface. This results in the preferential deposition of Pt nuclei at the defect sites and the further growth of these nuclei into Pt Nfs. Departure from local equilibrium at such defect sites may cause morphological instability and subsequent patterns, especially in the event of rapid solidification, to produce nanoflower growth.[69,70]

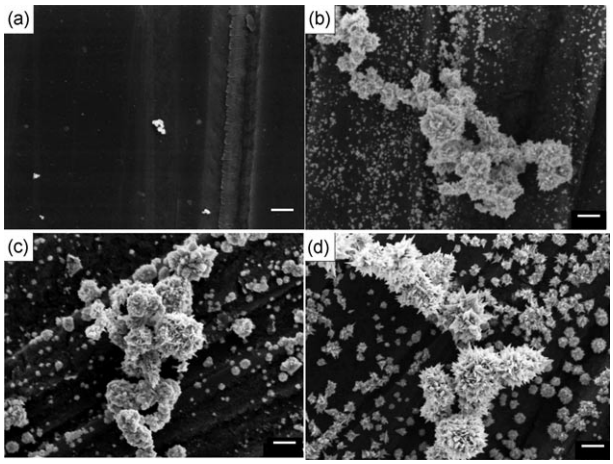


Figure 1. SEM images of Pt nanoflowers deposited on manually scratched silicon (#1000) by galvanic displacement. Bar: 100 nm. Galvanic deposition of Pt on the silicon substrates from an aqueous solution of 1 mM $H_2PtCl_6$ containing 5 M HF at different immersion times of a) 3 min, b) 10 min, c) 30 min, d) 60 min. Scale bars = 300 nm.

The morphology of the Pt Nfs is expected to depend on the growth conditions. Thus, we examined the effect of the following factors on the morphology of the Pt Nfs: 1) surface roughness of the scratched silicon and 2) concentration of the Pt ions. The surface roughness was varied by mechanical grinding of the silicon wafer with different scratching plates (#400, #1000, and #4000). The arithmetic mean deviations ($R_a$) of the profiles of the scratched silicon wafers were estimated to be 329 nm, 169 nm, and 61 nm, respectively, by confocal scanning laser microscopy (CSLM). From the SEM images of the Pt Nfs on scratched silicon surfaces with various degrees of roughness, it is apparent that the morphology of the Pt Nfs is almost independent of the surface roughness. This, in turn, suggests that surface roughness (i.e., degree of scratching) is not an important factor affecting the morphology of the Pt Nfs (see the Supporting Information, S1).

In contrast, the morphology of the Pt Nfs does depend on the concentration of $H_2PtCl_6$. Figure 2 compares the morphologies of the Pt particles formed on a scratched silicon wafer (#1000) by galvanic deposition from aqueous $H_2PtCl_6$ solutions of different concentrations (0.2 mM and 10 mM); the deposition time in this case was 10 min. The Pt particle density clearly increased with the $H_2PtCl_6$ concentration. More importantly, the morphology of the Pt particles changed from one of nanoflowers (1 mM, Figure 1a; 0.2 mM,

  

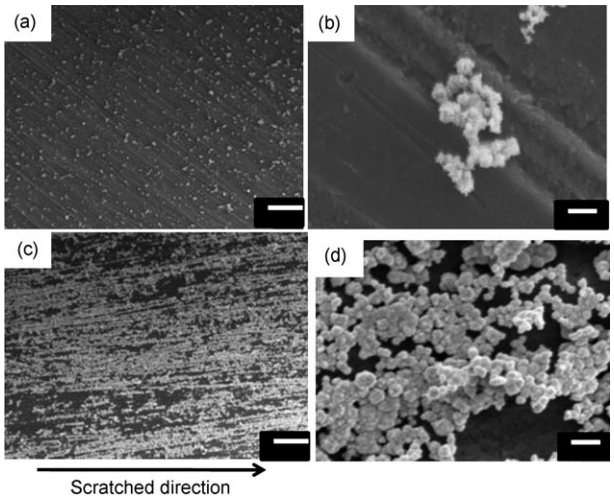


Figure 2. SEM images of Pt nanoflowers formed on manually scratched silicon (#1000) by galvanic displacement (immersion time: 10 min). Galvanic deposition of Pt on the silicon substrates from an aqueous solution containing 5 M HF and different concentrations of $H_2PtCl_6$: a) and b) 0.2 mM; c) and d) 10 mM. Scale bars: a) and c) 20 μm; b) and d) 300nm.

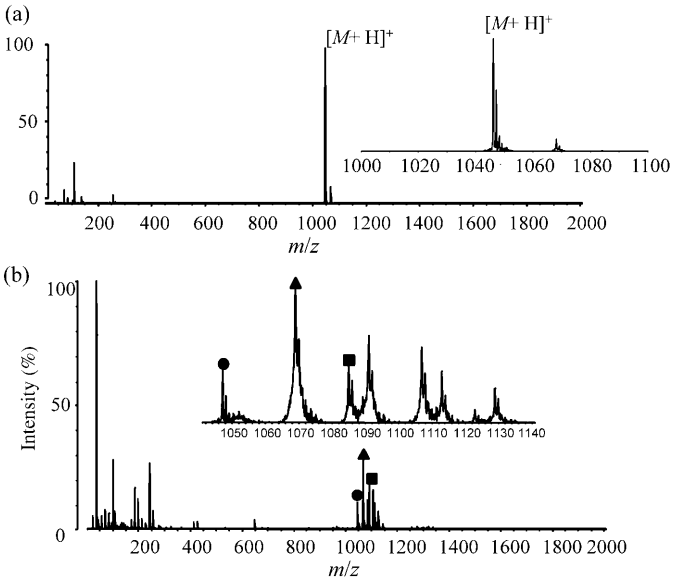


Figure 3. a) SALDI mass spectrum of angiotensin II (5 pmol) obtained using Pt nanoflowers on manually scratched silicon (#1000) in positive-ion mode. Galvanic deposition of Pt on the silicon substrates from an aqueous solution of 1 mM $H_2PtCl_6$ and 5 M HF (immersion time: 10 min). b) SALDI mass spectrum of angiotensin II (5 pmol) obtained using the manually scratched silicon in positive-ion mode. ●=$[M+H]^+$, ▲=$[M+Na]^+$, ■=$[M+K]^+$.

Figure 2b) to disc-like particles (10 mM, Figure 2d) as the concentration of $H_2PtCl_6$ was increased. At 10 mM, parallel rows of Pt particles were observed in the scratching direction (Figure 2c), implying scratching-induced Pt deposition on the silicon surface. Thus, it is likely that the growth of Pt Nfs on the scratched silicon substrate occurs when the $H_2PtCl_6$ concentration is at least in the range 0.1–1 mM.

Signal enhancement was achieved for protonated molecular ions in the SALDI mass spectra of peptides when using the Pt Nf silicon hybrid plate. In the above subsection, we presented the galvanic deposition of 3D Pt Nfs on scratched silicon (to obtain a Pt Nf silicon hybrid plate). The galvanic deposition time was set to 10 min because in our previous study we found that longer deposition times caused significant background noise in the SALDI mass spectra using spherical Pt particles on unscratched silicon.[70] Additionally, the dramatic decrease in silicon surface area by the surface modification is unfavorable for SALDI-MS. In this study, angiotensin II was chosen as a model peptide, and the SALDI performance was evaluated when using the Pt Nf silicon hybrid plate (Figure 1b); angiotensin II is typically used for preliminary screening when investigating the SALDI sensitivity for peptides. For comparison, the SALDI performance when using a scratched silicon plate without Pt deposition was also examined. As shown in Figure 3a), when using the Pt Nf silicon hybrid plate and 0.1% trifluoroacetic acid (TFA; proton source), the obtained mass spectra showed only peaks attributable to the protonated molecular ion of the peptide. The SALDI mass spectrum showed low chemical background noise in the low-mass region ($m/z<500$). In contrast, the mass spectrum obtained when using the scratched silicon plate without Pt deposition showed peaks corresponding to sodium and potassium adduct ions of the peptides and unknown ions, in addition to peaks corresponding to the protonated ions, irrespective of the presence of the TFA proton source (Figure 3b). High chemical background noise was also observed in the low-mass region ($m/z<300$). These results indicate that the hybridization of Pt Nfs with the silicon substrate enhances the efficiency of protonation of the peptide molecular ions in SALDI. Our previous study indicated that the deposition of Pt Nfs from a suitable suspension onto a MALDI plate (i.e., stainless steel plate) was inefficient for producing protonated species in the absence of a citrate buffer additive.[42,63] Thus, Pt Nfs alone cannot enhance the protonation of peptide molecular ions in SALDI. Combining Pt Nfs with the silicon substrate is important for generating protonated molecular ions.

The chemical state of the Pt–silicon interface formed during the deposition of Pt on the silicon surface may be important for charge separation of the electron/hole pair between silicon and Pt. To examine the chemical state of the Pt–silicon interface, we performed X-ray photoelectron spectroscopy (XPS) measurements on the Pt Nf silicon hybrid plate. Figure 4 shows the X-ray photoelectron spectra of the Pt 4f region for the Pt Nfs silicon plate, which was prepared by immersing a silicon substrate scratched with sandpaper (#1000) in an aqueous solution containing 1 mM $H_2PtCl_6$ and 5 M HF for deposition times of a) 10 s and b) 10 min. Pt $4f_{7/2}$ and $4f_{5/2}$ doublet peaks are seen in the spectrum. When the Pt deposition time was short (10 s), the Pt $4f_{7/2}$ peak in the obtained spectrum was further split into two peaks: one at 71.1 eV and the other at 72.8 eV. The former peak indicates the presence of metallic Pt, whereas the latter is indicative of platinum silicide (PtSi). These re-

  

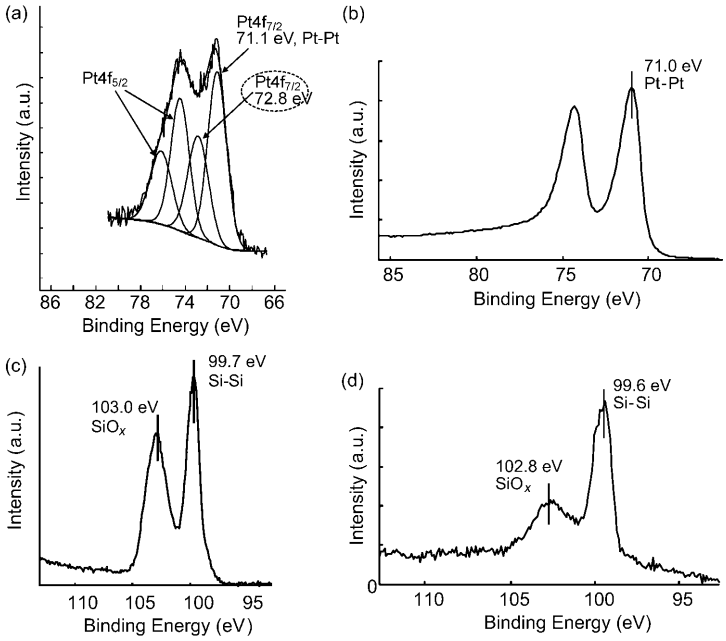


Figure 4. a) and b) XPS Pt 4f spectra obtained for Pt nanoflowers on manually scratched silicon (#1000). Galvanic deposition of Pt on the silicon substrates was from a 1 mM aqueous solution of $H_2PtCl_6$ containing 5 M HF for immersion times of 10 s (a) and 10 min (b). c) and d) XPS Si 2p spectra measured for Pt nanoflowers on manually scratched silicon (#1000). Galvanic deposition of Pt on the silicon substrates from a 1 mM aqueous solution of $H_2PtCl_6$ containing 5 M HF for immersion times of 10 s (c) and 10 min (d).

sults suggest that the Pt is well adhered to the silicon substrate because of the formation of PtSi. Recently, similar observations on PtSi formation have been reported for Pt galvanic deposition on unscratched silicon.[69] When the immersion time was short, the size of the deposited Pt nanoparticles was small. Thus, the XPS provides information about the interface between the deposited Pt metal and the silicon substrate. When the deposition time was long (10 min), only peaks due to the Pt metal present near the Pt Nf surface were observed in the XPS; the Pt $4f_{7/2}$ peak appeared at 71.0 eV. The close contact between the n-type silicon substrate and Pt interface owing to PtSi formation may be important for transferring the UV-irradiation-induced electrons from the silicon to the deposited Pt; this would result in near-surface hole-trapping on the silicon surface and a consequent increase in the acidity of the Si–OH groups.

The presence of $SiO_x$ was confirmed by XPS. The spectra of the Si 2p region for the Pt Nf silicon hybrid plate were recorded for deposition times of 30 s and 10 min, as shown in Figure 4c) and d), respectively. In the Si 2p region, two main peaks are visible in each spectrum: one attributable to silicon at 99.7 eV and the other attributable to $SiO_x$ at 102.8 eV, from $SiO_x$ that was probably formed by the oxidation of silicon, as the Pt Nf silicon hybrid plate was exposed to air for a short time before being placed in the XPS chamber. Similar oxidation of the Pt Nf silicon hybrid plate may have occurred prior to the SALDI-MS experiments. The Pt/Si XPS ratio increased from 0.3 (deposition time: 30 s) to 12.7 (deposition time: 10 min), confirming the growth of Pt on silicon by galvanic deposition.

On the basis of the above-mentioned hypothesis, we state that Pt nanoparticle deposition helps to enhance the protonation of molecular ions not only when employing silicon substrates but also when employing other UV-absorbing semiconductor materials. Similar to silicon, $TiO_2$ also acts as a semiconductor and is a promising SALDI-MS substrate because of its high UV absorbance and high chemical stability. However, $TiO_2$ nanomaterials have been reported to be inefficient for producing protonated species for SALDI-MS in the absence of a citrate buffer additive.[19,37–39] The deposition of Pt nanoparticles on a $TiO_2$ surface is known to suppress electron hole/pair recombination.[71,72] Thus far, studies on enhanced charge separation on Pt-decorated $TiO_2$ surfaces have focused extensively on photocatalysis. Effective UV-irradiation-mediated charge separation on Pt-decorated $TiO_2$ surfaces would help in the production of protonated species in SALDI-MS, as in the case of using the Pt-decorated silicon substrates. To confirm this possibility, we examined the effectiveness of Pt nanoparticle deposition on a $TiO_2$ nanotube array (TNA). SEM images revealed the porous morphologies of the TNA and the Pt-decorated TNA substrate (see the Supporting Information S2). The SALDI mass spectra of a peptide mixture (Des-ArgI-Bradykinin, angiotensin I, and neurotensin) were obtained using the TNA and Pt-decorated TNA substrate. Peaks due to the protonated molecular ions of the peptides (5 pmol) could be detected in the spectrum when using the Pt-decorated TNA plate along with 0.1% TFA; on the other hand, when using the TNA plate, peaks due to these ions could not be detected in the absence of citrate buffer additives (Supporting Information S2). These results confirm that Pt nanoparticle deposition is effective for enhancing the protonation of molecular ions in $TiO_2$-based and silicon-based SALDI-MS.

**Laser threshold for SALDI-MS when using the Pt Nf silicon hybrid plate**: The minimum laser energy required to generate stable ion signals (i.e., the laser threshold) is an important benchmark for characterizing the effectiveness of MALDI,[73] SALDI,[23,61] and DIOS.[58,74] In this study, we examined the laser threshold for angiotensin II and GGYR in SALDI-MS when using a Pt Nf silicon hybrid plate and a disc-like Pt Nf silicon hybrid plate (shown in Figure 2d). The laser threshold was found to be smaller when using the Pt Nf silicon hybrid plate (20 mJ cm$^{-2}$ for angiotensin II and 25 mJ cm$^{-2}$ for GGYR) than when using the disc-like Pt silicon hybrid plate (94 mJ cm$^{-2}$ for angiotensin II and 67 mJ cm$^{-2}$ for GGYR). The smaller laser threshold in the former case suggests the importance of the Pt Nf morphology in enhancing the efficiency of peptide desorption/ionization. In a previous study, we suggested that Pt Nfs can efficiently absorb energy during desorption and that the morphological features of the Pt Nfs, such as the roughness and porosity generated by the formation of petals and the tip sharpness of the petals on the surface, are very important in improving the SALDI performance.[42] Among these factors,

  

we consider the tip sharpness of the petals on the surface to be effective for increasing the laser-induced temperature; this is because of the low thermal conductivity and thermal conferment of the Pt Nfs. As a result, a low laser fluence is sufficient to ensure that the Pt Nfs attain the same temperature as the disc-like Pt Nfs. A similar low laser threshold has been reported for SALDI-MS employing silicon nanowires grown on silicon surfaces.[74]

As mentioned above, we prepared Pt Nf silicon hybrid plates with the desired surface roughness by mechanical grinding of the silicon wafer (SEM images shown in the Supporting Information S1). For all of the Pt Nf silicon hybrid plates, the mass spectra showed peaks due to the protonated molecular ion of angiotensin II when 0.1% TFA was used. A small laser threshold was required for Pt Nf silicon hybrid plates with higher surface roughness (see the Supporting Information S3). This is consistent with previous reports, according to which a small laser threshold is required to produce ions on a silicon substrate with high porosity or a large total surface area.[14] However, in contrast to the mass spectra obtained when using the silicon hybrid plates prepared by manual grinding (Figure 3a), those obtained when using the Pt Nf silicon hybrid plates prepared by mechanical grinding showed a number of unknown signals in the low-mass region. Since the spectra obtained for the mechanically ground hybrid plate included chemical background noise, we used the Pt Nf silicon hybrid plate produced by manual grinding of the silicon wafer with sandpaper (#1000) for the following SALDI-MS studies.

**Survival yield measurements of thermometer ions on the Pt Nf silicon hybrid plate**: In the SALDI process, excess energy may be transferred to individual molecules, and this may lead to undesired fragmentation, as opposed to the soft desorption in MALDI. To examine the degree of internal energy transfer in the desorption process, we measured the survival yield (SY) of a model substance, benzylpyridine (BP), which affords a series of benzylpyridinium ions, the so-called "thermometer ions" (TM). Details of the SY method using TM ions have been previously reported in the literature.[57,59,61,64,76] We performed SY measurements on BP-Cl by SALDI-MS using the Pt Nf silicon hybrid plate. To further improve the SALDI efficiency in terms of sensitivity[58] and soft desorption,[61] we modified the Pt Nf silicon hybrid plate by derivatizing the surface OH groups of the substrate with FDTS. The reaction time for FDTS silylation was set at 5 h to avoid morphological changes in the Pt Nfs. When the reaction time was increased to 24 h, a dramatic morphological change in the Pt Nfs was observed (Supporting Information S4). The SALDI mass spectrum of BP-Cl exhibits two primary peaks: a molecular ion $M^+$ peak ($m/z$ 204) and the corresponding fragment $F^+$ peak (benzyl cation, $m/z$ 125), as shown in Figure 5a). The SY value is determined according to Equation (1):

$$\mathrm{SY} = \frac{I_\mathrm{M}}{(I_\mathrm{M} + I_\mathrm{F})} \qquad (1)$$

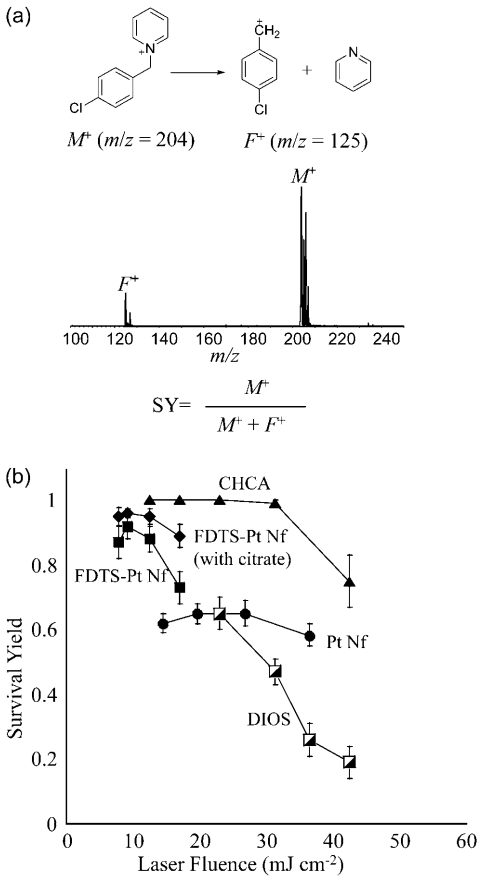


Figure 5. a) SALDI mass spectrum of BP-Cl using Pt nanoflowers (Pt Nfs) on manually scratched silicon (#1000). b) Comparison of molecular ion survival yields of BP-Cl in SALDI-MS using Pt Nfs, FDTS-modified Pt Nfs, FDTS-Pt Nfs (with citrate buffer), DIOS, and MALDI with CHCA matrix.

in which $I_\mathrm{M}$ and $I_\mathrm{F}$ are the experimentally measured intensities of the $M^+$ and $F^+$ peaks, respectively. The internal energy is inversely proportional to the SY. The change in the SY of BP-Cl with laser fluence was also examined. For comparison, SY measurements were also carried out for DIOS with CHCA in MALDI.

As shown in Figure 5b), in the case of the Pt Nf silicon hybrid plate, the threshold for ion production was reached at a low laser fluence (14 mJ cm$^{-2}$), which is comparable with that in MALDI (13 mJ cm$^{-2}$). Although the SY values of the Pt Nf silicon hybrid plate ($\approx$0.65) are lower than those observed in the MALDI process (SY$\approx$1), the FDTS-modified Pt Nf silicon hybrid plate (FDTS-Pt Nf silicon) has a major impact on the increase in the SY values ($\approx$0.92), that is, the decrease in the degree of fragmentation. The addition of citrate buffer further increased the SY ($\approx$0.97) of the FDTS-Pt Nf silicon plate. This suggests that surface modification by fluorinated chains helps to decrease the internal energy during analyte desorption from the surface. One possible reason for this is as follows: the weak interaction of the surface-fluorinated chains with BP-Cl may lead to a decrease in the energy barrier for analyte desorption

  

from the surface (i.e., an increase in the SY value). Another possible reason for the high SY of the FDTS-Pt Nf silicon hybrid plate is non-thermal desorption. The laser-induced explosive evaporation of the surface-fluorinated chains may help to desorb the BP-Cl and ensures that the critical energy for surface desorption is lower than that for simple thermal desorption. Note that the SY values (i.e., fragmentation behavior) change significantly with the laser fluence in the case of the FDTS-Pt Nf silicon hybrid plate. This implies the possibility of secondary molecular collisions in the gas phase, during which energy exchange occurs.[14] Co-desorption of the fluorinated chains and BP-Cl ions at a high laser fluence allows molecular collisions in the gas phase between these species; hence, the SY values decrease at a high laser fluence.[14] In contrast, for the Pt Nf silicon hybrid plate, the SY values remain practically unchanged in the examined fluence range because there is no co-desorption of the surface-modified molecules and BP-Cl ions.

Surface reconstruction/destruction or melting of the SALDI substrate upon laser irradiation can contribute to non-thermal desorption and thus trigger the desorption process.[62–64] Since the melting temperature of nanosized metals is lower than that of bulk metals, deformation or ablation of Pt nanostructures may occur during irradiation by a pulsed laser. Therefore, we observed the structure of Pt Nfs after laser irradiation at 50 mJ cm$^{-2}$, which is sufficient for detecting peptides by SALDI-MS. The SEM images demonstrated that there was very little change in the morphology of the Pt Nfs after laser irradiation (see the Supporting Information S5). Therefore, surface reconstruction/destruction of Pt Nfs upon laser irradiation may contribute to a small extent to non-thermal desorption for triggering the SALDI process. This suggests that in the case of the Pt Nf silicon hybrid plate and the FDTS-Pt Nf silicon hybrid plate, SALDI activity can be observed at a laser energy lower than the laser threshold for surface reconstruction/destruction or melting.

**Durability of FDTS-Pt Nf silicon hybrid plates**: The SALDI activity of silicon has been reported to decay after a few days of exposure to ambient air.[16] However, we did not observe any such degradation for the Pt Nf silicon hybrid plate even when it was exposed to air. Good quality signals were obtained from angiotensin II when using a one-month-old plate, and the laser threshold was 23 mJ cm$^{-2}$ (see the Supporting Information S6). Degradation of the Pt Nf silicon hybrid plate upon exposure to ambient air was mainly indicated by the appearance of unknown peaks in the mass spectra at $m/z < 100$ and peaks due to sodium and potassium ions, which were probably formed by air contamination.

**Applicability of FDTS-Pt Nf silicon hybrid plate to various analytes**

*Phospholipids*: When using the FDTS-Pt Nf silicon hybrid plate, a high SY was observed for molecular ions at a low laser fluence. For this reason, we consider that the FDTS-Pt Nf silicon hybrid plate should have potential application in the SALDI-MS analysis of labile compounds. We selected a phospholipid as a model labile compound. In the detection of phospholipids by a SALDI process, such as DIOS, peaks due to the fragment ions obtained from the polar head group are predominantly observed in the mass spectrum, while the molecular ion peak is indistinct. However, such fragment ion peaks are not predominant in the spectrum when phospholipids are analyzed by MALDI-MS using a typical chemical matrix such as DHBA. This suggests that the ionization conditions in SALDI-MS are harsher than those in MALDI-MS. In this study, we found that the FDTS-Pt Nf silicon hybrid plate showed a relatively lower fragmentation tendency. Figure 6 shows the mass spectra of DMPC obtained when using the Pt Nf silicon hybrid plate and the FDTS-Pt Nf silicon hybrid plate, in addition to the MALDI spectra obtained with DHBA. The spectrum obtained using the Pt Nf silicon hybrid plate shows peaks corresponding to the lipid molecular ions $[M+Na]^+$and $[M+H]^+$, but peaks due to the fragments ($m/z$ 184 and 86) from the polar head group are still predominant (Figure 6a).

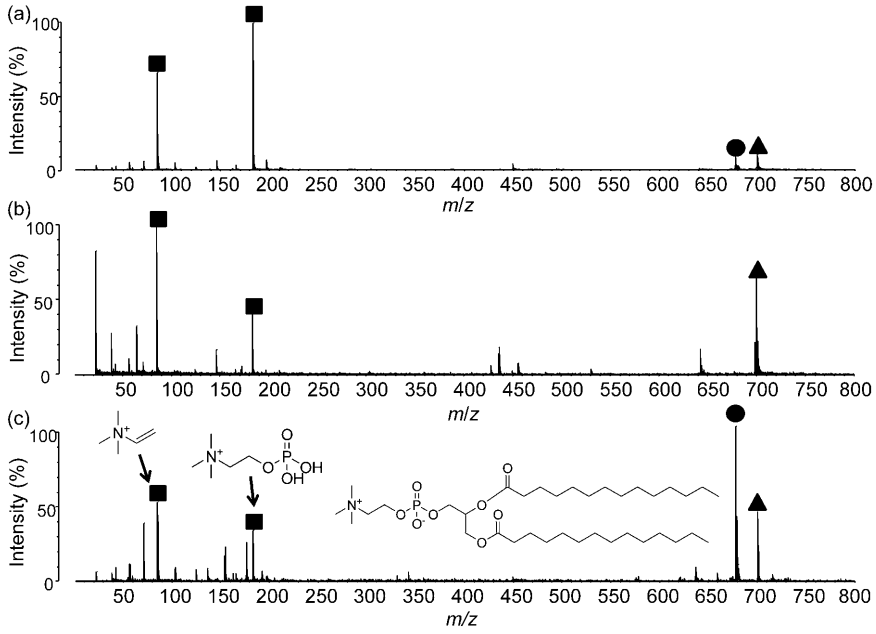


Figure 6. SALDI mass spectra of DMPC (60 pmol) in the presence of 0.5 mM NaTFA using a) Pt nanoflowers (Pt Nfs) on manually scratched silicon (#1000), b) FDTS-modified Pt Nfs, and c) MALDI with DHBA matrix. ● = $[M+H]^+$, ▲ = $[M+Na]^+$, ■ = fragment ion.

In contrast, the mass spectrum obtained using the FDTS-Pt Nf silicon hybrid plate clearly shows peaks due to the lipid molecular ion $[M+Na]^+$; from the spectrum, it is apparent that the degree of fragmentation becomes low (Figure 6b), comparable to that observed in the MALDI process with DHBA (Figure 6c).

*Synthetic polymers*: Polyethylene glycol (PEG) is used in a number of pharmaceutical, industrial, and food additive applications, for example laxatives, skin creams, personal lubricants, toothpastes, and thickening agents; binding agents for ceramic molds, casting, and powder metallurgy; oligomers for polyurethane manufacture; and non-ionic detergents. Recently, we reported that fragment ions with $m/z$ 500–3000 are predominantly generated in the $TiO_2$-SALDI of PEG 6000; however, no precursor ions ($m/z \approx 6000$) are formed in this case.[39] Further, in SALDI-MS using Au nanoparticles, PEG fragment ions with molecular weights of more than 3000 are predominantly formed, and precursor ions are also observed.[63] It has been reported that $EuF_3$ microdiscs with hollow interiors can be successfully used for the detection of PEG precursor ions with molecular weights up to 30000, although the fragmentation pattern is still not clear.[53] Precursor ions of PEG 6000 have also been detected in ZnO-SALDI, in which the degree of fragmentation is low.[36] In this study, we performed a SALDI-MS analysis of PEG 6000 by using the FDTS-Pt Nf silicon hybrid plate. The SALDI mass spectrum of PEG 6000 showed peaks due to the precursor ions with a molecular weight distribution around $m/z$ 6000 with little fragmentation (Figure 7b), similar to the MALDI mass spectrum obtained with CHCA (Figure 7a). The FDTS-Pt Nf silicon hybrid plate was also effective for the analysis of hydrophobic polymers, such as poly(methyl methacrylate) (PMMA), as shown in Figure 7d); this was because high-molecular weight PMMA ions could be detected at a laser power lower than that required for MALDI (Figure 7c). Thus, the performance achieved with the FDTS-Pt Nf silicon hybrid plate was comparable to that achieved in MALDI in terms of the molecular weight distribution of the polymer ions and limited fragmentation.

*Peptides, carbohydrates, and small molecules*: The use of the FDTS-Pt Nf silicon hybrid plate helps to improve the detection sensitivity for peptides, carbohydrates, and small molecules (see the Supporting Information S7). When using the

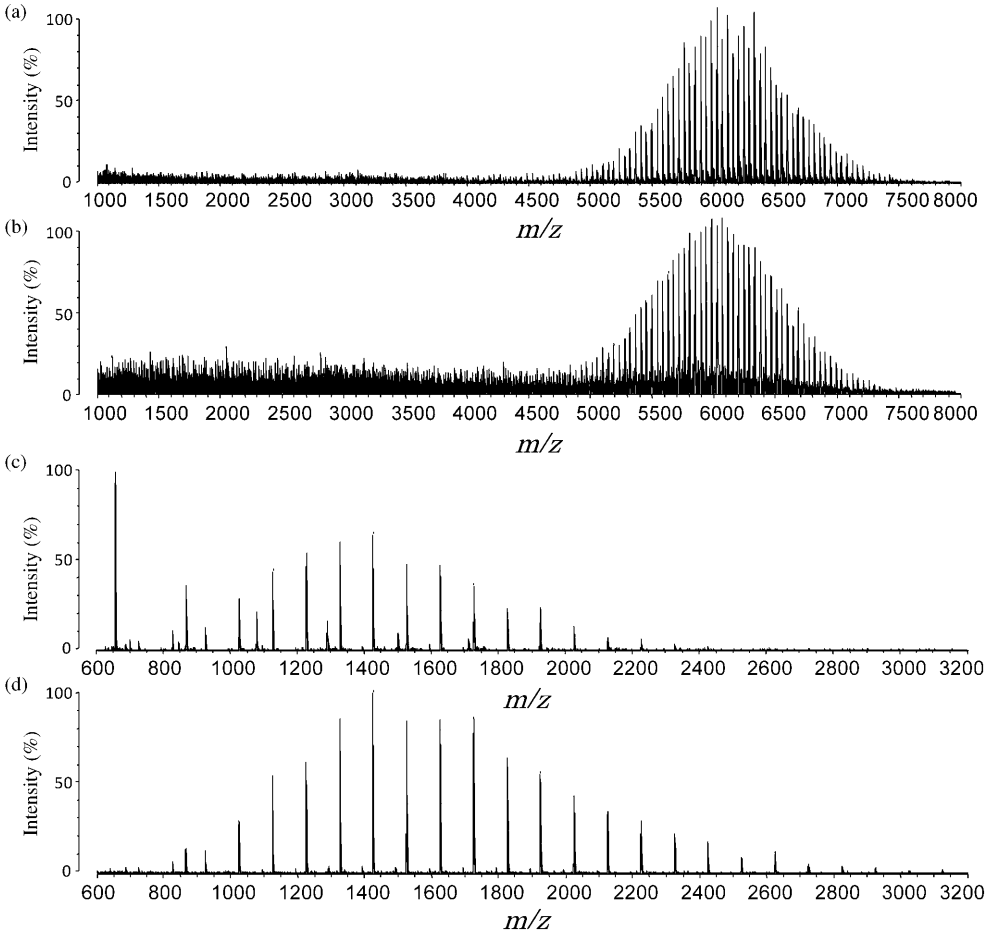


Figure 7. Mass spectra of PEG 6000 (1 mg mL$^{-1}$) in the presence of 0.5 mM NaTFA using a) MALDI with CHCA matrix and b) FDTS-modified Pt Nfs. LDI mass spectra of PMMA (1 mg mL$^{-1}$) in the presence of 0.5 mM NaTFA using c) MALDI with CHCA matrix and d) FDTS-Pt Nfs.

  

FDTS-Pt Nf silicon hybrid plate, the minimum amount of angiotensin II and GGYR samples required for obtaining spectra with reasonable signal-to-noise ratios was about 5 fmol in the absence of citrate buffer. The detection limits for β-cyclodextrin and caffeine (500 fmol and 10 pmol, respectively) are relatively lower than those for angiotensin II and GGYR. For amine-containing drugs, such as verpamil hydrochloride, the detection limit is 5 fmol. However, the detection of small acidic drug molecules, such as deprotonated aspirin and vitamin C proved impossible by SALDI-MS when using the FDTS-Pt Nf silicon hybrid plate, even at high concentrations (100 pmol) of the analytes (see the Supporting Information S8). The detection of deprotonated ions in negative-ion mode is very difficult when using the FDTS-Pt Nf silicon hybrid plate, probably because of the surface chemical properties of the plate. The silicon oxide surface is intrinsically acidic because of the chemical properties of the terminal Si–OH groups, as in the case of DIOS chips.[77] The acidity of the Si–OH moieties may be further increased because of the electron-withdrawing nature of the surface fluorocarbon chains and Pt particles on the silicon plate. Therefore, the analytes deposited on the surface are in an acidic environment; this results in differences in the degree of deprotonation of acidic compounds. On the other hand, increased surface basicity may facilitate the formation of negative ions from small acidic molecules. In fact, we reported in a previous paper that a polyethyleneimine-modified graphite substrate is suitable for the effective detection of the deprotonated ions of perfluorooctanoic acid in negative-ion mode.[32]

**On-plate phosphopeptide enrichment using FDTS-Pt Nf silicon hybrid plates**: The selective detection of phosphopeptides from proteolytic digests is of very high relevance in many proteomics applications. In proteolytic digests, phosphopeptides are often present in small amounts. The coexistence of non-phosphopeptides decreases the peak ion intensity of phosphopeptides in the LDI mass spectra because of the efficient LDI of the non-phosphopeptides (the so-called ion-suppression effect). Therefore, selective isolation and/or enrichment of phosphopeptides from a mixture is essential before identification by LDI-MS. Thus, to date, $TiO_2$ materials have been employed for the enrichment of phosphopeptides from complex mixtures because of the specific affinity of $TiO_2$ for phosphopeptides.[26,41] Here, we found that the FDTS-Pt Nf silicon hybrid plate could be used for the enrichment of phosphopeptides by direct SALDI-MS analysis. The following peptide mixture containing ten kinds of non-phosphopeptides (allanton, angiotensin fragment 1–7, RASG-1, angiotensin II, bradykinin, angiotensin I, renin substrate, enolase T35, enolase T37, and melittin) and four kinds of phosphopeptides (T181-1P, T191-1P, T43-1P, and T43-2P) was used in this study. The molecular weights of these peptides are summarized in Table S1 in the Supporting Information. Figure 8a) presents the SALDI mass spectrum of the peptide mixture containing phosphopeptides before the washing treatment. Among the four spiking phosphopeptides used, only one showed a weak peak ($m/z$ 1369.7) in the mass spectrum, which corresponded to the protonated molecular ion (Figure 8a). This indicated that the signals due to the phosphopeptides were completely suppressed in the SALDI mass spectrum. Peptides with high molecular weights, such as renin substrates, enolase T35, enolase T37, and melittin were not detected. When the FDTS-Pt Nf silicon hybrid plate was subjected to washing procedures, peaks due to all of the phosphopeptides could be seen in the SALDI mass spectrum (Figure 8b). This result indicates that the FDTS-Pt Nf silicon hybrid plate has some affinity for phosphopeptides, and hence, this plate can be used for the enrichment of phosphopeptides from mixtures. However, the reason for this affinity is not clear at present. The interaction of phospholipid (Lewis base) with Pt Nfs (Lewis acid) might contribute to the on-plate phosphopeptide enrichment.

To further confirm the phosphopeptide-trapping capacity of the FDTS-Pt Nf silicon hybrid plate, we used the tryptic digest product of β-casein as a sample; this is because β-casein is a commonly used phosphoprotein. Peaks corresponding to phosphopeptides from the tryptic digest product of β-casein were detected at $m/z$ 2062, 2556, and 3122 only when using the washed PFD-Pt Nf silicon hybrid plate (Figure 8c, d). The phosphopeptides identified are summarized in Table S2 in the Supporting Information. The results indicated that the PFD-modified Pt Nf silicon hybrid plate acted as an affinity substrate for phosphopeptides and as a SALDI substrate, which is similar to the affinity work on $TiO_2$ substrates. By optimizing the extraction and washing steps, the procedure will be further improved.

## Conclusion

We have reported for the first time the fabrication of 3D Pt nanoflowers (Pt Nfs) on a scratched silicon substrate by electroless galvanic displacement and the application of these Pt Nfs in SALDI-MS. Surface scratching is essential to induce Pt Nf growth on the silicon substrate (to obtain a Pt Nf silicon hybrid plate) by galvanic displacement. Surface scratching of the silicon wafer produces defect sites, such as step edges, pits, and dangling bonds on the silicon surface, and hence preferential deposition of the Pt nuclei occurs at the defect sites. These Pt nuclei can then be grown into Pt Nfs. When there is supersaturation at such defect sites, morphological instability can occur, and nanoflower-like growth forms may appear.

Using this Pt Nf silicon hybrid plate, we achieved excellent SALDI activity in terms of the efficient generation of protonated molecular ions in the absence of a citrate buffer. The acidity of the Si–OH moieties on the silicon increases because of the electron-withdrawing nature of the Pt Nfs. As a result, proton transfer from the Si–OH groups to the analyte molecules is enhanced, and there is thermal desorption of the analyte ions from the surface. Signal enhancement of protonated molecular ions has also been observed

  

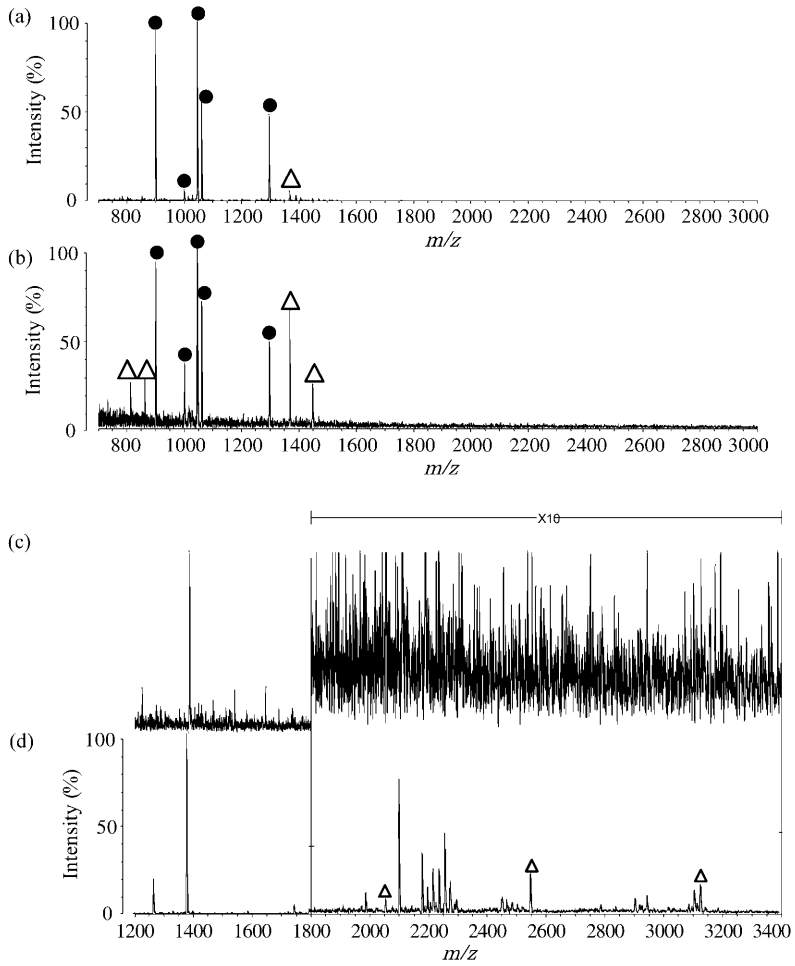


Figure 8. SALDI mass spectra of the peptide mixture containing phosphopeptides a) before and b) after washing treatment. A peptide mixture containing ten kinds of non-phosphopeptides (●; allanton, angiotensin fragments 1–7, RASG-1, angiotensin II, bradykinin, angiotensin I, renin substrate, enolase T35, enolase T37, and melittin) and four kinds of phosphopeptides (△; T181-1P, T191-1P, T43-1P, and T43-2P) was used. SALDI mass spectra of the tryptic digest product of β-casein c) before and d) after washing treatment.

for a $TiO_2$ nanotube array substrate upon photochemical deposition of Pt nanoparticles.

Surface modification of the Pt Nf silicon hybrid plate by FDTS (an FDTS-Pt Nf silicon hybrid plate is obtained as a result) helps to improve the detection sensitivity for peptides, carbohydrates, and small molecules. Another advantage of using the FDTS-Pt Nf silicon hybrid plate is the soft SALDI process, which has been demonstrated by the survival yields of a thermometer ion (BP-Cl). As a result, by using the FDTS-Pt Nf silicon hybrid plate, labile compounds, such as phospholipids and PEG 6000, can be detected with a very low degree of fragmentation in SALDI-MS. The feasibility of using FDTS-Pt Nf silicon hybrid plates (or Pt Nf silicon hybrid plates) for matrix-free SALDI-MS analysis has been demonstrated by using a β-casein digest and various analytes, including small molecules, peptides, phosphopeptides, phospholipids, carbohydrates, and synthetic polymers. More importantly, we have found for the first time that the FDTS-Pt Nf silicon hybrid plate acts as an affinity substrate for phosphopeptides as well as a SALDI substrate.

The Pt Nf silicon hybrid plate may be readily extended to other transition metals, such as palladium and rhodium, and efforts towards achieving this are in progress in our laboratory. The study is of significance in shape-controlled synthesis of metal nanoparticles, and is of importance not only with regard to SALDI applications, but also surface-enhanced Raman scattering (SERS), electrocatalysis, sensors, and fuel cells.[76–78]

## Experimental Section

**Preparation of Pt Nfs on scratched silicon by galvanic displacement**: A silicon wafer was cut into 1.5 cm × 1.5 cm squares and sonicated in acetone and methanol for 10 min each. Scratched silicon wafers were produced by two methods: i) manual grinding of the silicon wafer by using sandpaper (#1000) and ii) mechanical grinding of the silicon wafer with a grinding machine (Marumoto Struers S5629) and different wet SiC papers of #400, #1000, and #4000 (Marumoto Struers) for 60 s. During mechanical grinding, the rotation speed of the papers was adjusted to 50 rpm. The scratched silicon wafer was sonicated in acetone and methanol for 10 min and then etched with 46% HF for 20 min. Typically, electroless galvanic deposition of Pt Nfs on the silicon surface was carried out by immersing the scratched silicon substrate in a 1 mM aqueous solution of $H_2PtCl_6$ containing 5 M HF for 10 min. After immersion, the silicon substrate was washed with water and preserved in EtOH until further use in the SALDI-MS experiments.

Caution! HF is a hazardous acid that can cause serious tissue damage if burns are not appropriately treated. Thus, HF should be handled in a well-ventilated fume hood while wearing appropriate chemical safety items: a face shield and double-layered nitrile gloves.

**Surface silylation of Pt Nf silicon hybrid plate**: The Pt Nf silicon hybrid plate was modified with FDTS or 3-aminopropyltrimethoxysilane (APTMS) via the surface OH groups on the substrate. The surface silylation reaction was induced by immersing the Pt Nf silicon hybrid plate in hexane containing 1 mM perfluorodecyltrichlorosilane (PFDS) for 5 h at 25 °C. Subsequently, the substrate was washed with excess hexane and then with EtOH.

**SALDI-MS**: The substrates prepared for SALDI-MS were fixed to a stainless steel sample plate using double-sided conductive carbon tape. The sample solution containing 0.5 μL of a cationization agent (0.1% TFA or 1 mM NaI) was spotted onto this substrate and dried under reduced pressure. SALDI mass spectra were obtained in linear mode by using an AXIMA CFR TOF mass spectrometer (Shimadzu, Kyoto,

  

Japan) fitted with a pulsed nitrogen laser (337 nm). One hundred laser shots were used to acquire the mass spectra. The analyte ions were accelerated at 20 kV under delayed extraction conditions.

**Survival yield (SY) measurements of thermometer ion**: Benzylpyridinium chloride (BP-Cl) was synthesized by the reaction of pyridine (anhydrous, purity > 99.8 %, Sigma Aldrich) and the corresponding substituted benzyl chloride (95–99 % pure, Sigma Aldrich).[64] Benzyl chloride was mixed with anhydrous pyridine (3 mL; pyridine/benzyl chloride molar ratio: 20:1), and this mixture was heated in a water bath for 5 h at 60 °C. Excess pyridine was removed by vacuum evaporation. The identities of the compounds with BP-Cl were confirmed by SALDI-MS analysis and used without further purification. A stock solution of BP-Cl (0.166 mM) was prepared in methanol.

## Acknowledgements

This study was partially supported by a Grant-in-Aid for Scientific Research (B) (Nos. 22350040 (to R.A.), 21310072 (to T.Y.)) from the Japan Society for the Promotion of Science (JSPS) and the Ministry of Education, Culture, Sports, Science and Technology (MEXT), Japan. T.Y. is also grateful for partial financial support from Grant-in-Aid for Scientific Research in Priority Area, "Molecular Science for Supra Functional Systems (477)" (No. 22018001) from MEXT. This research was partly supported by the Core-to-Core Program promoted by the Japan Society for the Promotion of Science (Project No. 18004). This study was supported by the "Strategic Project to Support the Formation of Research Bases at Private Universities": Matching Fund Subsidy from MEXT.

[1] K. Tanaka, H. Waki, Y. Ido, S. Akita, Y. Yoshida, T. Yoshida, *Rapid Commun. Mass Spectrom.* **1988**, *2*, 151.
[2] M. Karas, D. Bachmann, F. Hillenkamp, *Anal. Chem.* **1985**, *57*, 2935.
[3] a) M. W. F. Nielen, *Mass Spectrom. Rev.* **1999**, *18*, 309; b) S. D. Hanton, *Chem. Rev.* **2001**, *101*, 527; c) K. Deisewerd, *Chem. Rev.* **2003**, *103*, 395; d) M. Karas, R. Kruger, *Chem. Rev.* **2003**, *103*, 427; e) R. Knochenmuss, R. Zenobi, *Chem. Rev.* **2003**, *103*, 441.
[4] F. Hillenkamp, J. Peter-Katalinić, *MALDI-MS: A Practical Guide to Instrumentation, Methods and Applications, Small-Molecule Desorption/Ionization Mass Analysis*, Wiley-VCH, Weinheim, Chapter 9, **2007**.
[5] D. S. Peterson, *Mass Spectrom. Rev.* **2007**, *26*, 19.
[6] J. Wei, J. M. Buriak, G. Siuzdak, *Nature* **1999**, *399*, 243.
[7] R. A. Kruse, S. S. Rubakhin, E. V. Romanova, P. W. Bohn, J. V. Sweedler, *J. Mass Spectrom.* **2001**, *36*, 1317.
[8] Z. Shen, J. J. Thomas, C. Averbuj, K. M. Broo, M. Engelhard, J. E. Crowell, M. G. Finn, G. Siuzdak, *Anal. Chem.* **2001**, *73*, 612.
[9] E. P. Go, J. E. Prenni, J. Wei, A. Jones, S. C. Hall, H. E. Witkowska, Z. Shen, G. Siuzdak, *Anal. Chem.* **2003**, *75*, 2504.
[10] J. D. Cuiffi, D. J. Hayes, S. J. Fonash, K. N. Brown, A. D. Jones, *Anal. Chem.* **2001**, *73*, 1292.
[11] E. P. Go, J. V. Apon, G. Luo, A. Saghatelian, R. H. Daniels, V. Sahi, R. Dubrow, B. F. Cravatt, A. Vertes, G. Siuzdak, *Anal. Chem.* **2005**, *77*, 1641.
[12] G. Piret, H. Drobecq, Y. Coffinier, O. Melnyk, R. Boukherroub, *Langmuir* **2010**, *26*, 1354.
[13] N. H. Finkel, B. G. Pervo, O. D. Velev, L. He, *Anal. Chem.* **2005**, *77*, 1088.
[14] Y. Xiao, S. T. Retterer, D. K. Thomas, J.-Y. Tao, L. He, *J. Phys. Chem. C* **2009**, *113*, 3076.
[15] Y. Chen, A. Vertes, *Anal. Chem.* **2006**, *78*, 5835.
[16] S. Alimpiev, S. Nikiforv, V. Karavanskii, T. Minton, J. Sunner, *J. Chem. Phys.* **2008**, *128*, 014711.
[17] T. R. Northen, O. Yanes, M. T. Northen, D. Marrinucci, W. Uritboonthai, J. Apon, S. L. Golledge, A. Nordestrom, G. Siuzdak, *Nature* **2007**, *449*, 1033.
[18] C. T. Chen, Y. C. Chen, *Rapid Commun. Mass Spectrom.* **2004**, *18*, 1956.
[19] C. Y. Loa, J. Y. Lina, W. Y. Chena, C. T. Chena, Y. C. Chen, *J. Am. Soc. Mass Spectrom.* **2008**, *19*, 1014.
[20] M. J. Kang, J. C. Pyun, Y. J. Choi, J. H. Park, J. G. Park, J. G. Lee, H. J. Choi, *Rapid Commun. Mass Spectrom.* **2005**, *19*, 3166.
[21] M. Yuan, Z. Shan, B. Tian, B. Tu, P. Yang, D. Zhao, *Microporous Mesoporous Mater.* **2005**, 78, 37.
[22] T. Seino, H. Sato, A. Yamamoto, A. Nemoto, M. Torimura, H. Tao, *Anal. Chem.* **2007**, *79*, 4827.
[23] S. Okuno, R. Arakawa, K. Okamoto, Y. Matsui, S. Seki, T. Kozawa, S. Tagawa, Y. Wada, *Anal. Chem.* **2005**, *77*, 5364.
[24] R. Nayak, D. R. Knapp, *Anal. Chem.* **2007**, *79*, 4950.
[25] V. Jokinen, S. Aura, L. Luosujärvi, L. Sainiemi, T. Kotiaho, S. Franssila, M. Baumann, *J. Am. Soc. Mass Spectrom.* **2009**, *20*, 1723.
[26] H. Bi, L. Qiao, J. M. Busnel, V. Devaud, B. Liu, H. H. Girault, *Anal. Chem.* **2009**, *81*, 1177.
[27] H. Yan, N. Xu, W. Y. Huang, H. M. Han, S. J. Xiao, *Int. J. Mass Spectrom.* **2009**, *281*, 1.
[28] L. C. Chen, J. Yonehama, T. Ueda, H. Hori, K. Hiraoka, *J. Mass Spectrom.* **2007**, *42*, 346.
[29] a) H. Kawasaki, T. Sugitani, T. Watanabe, T. Yonezawa, H. Moriwaki, R. Arakawa, *Anal. Chem.* **2008**, *80*, 7524; b) A. Tarui, H. Kawasaki, T. Taiko, T. Watanabe, T. Yonezawa, R. Arakawa, *J. Nanosci. Nanotechnol.* **2009**, 9, 159.
[30] M. Hong, F. Qiu, L. L. Huang, J. Zhu, *J. Phys. Chem. C* **2008**, *112*, 11078.
[31] M. Najam-ul-Haq, M. Rainer, C. W. Huc, P. Hausberger, H. Kraushaar, G. K. Bonn, *Anal. Chem.* **2008**, *80*, 7467.
[32] H. Kawasaki, N. Takahashi, H. Fujimori, K. Okumura, T. Watanabe, C. Matsumura, S. Takemine, T. Nakano, R. Arakawa, *Rapid Commun. Mass Spectrom.* **2009**, *23*, 3323.
[33] T. Yalcin, L. Li, *Appl. Surface Sci.* **2009**, *256*, 1309.
[34] J. Sunner, E. Dratz, Y. C. Chen, *Anal. Chem.* **1995**, *67*, 4335.
[35] M. V. Ugarov, T. Egan, D. V. Khabashesku, J. A. Schultz, H. Peng, V. N. Khabashesku, H. Furutani, K. S. Prather, H. W. J. Wang, S. N. Jackson, A. S. Woods, *Anal. Chem.* **2004**, *76*, 6734.
[36] T. Watanabe, H. Kawasaki, T. Yonezawa, R. Arakawa, *J. Mass Spectrom.* **2008**, *43*, 1063.
[37] C. T. Chen, Y. C. Chen, *Anal. Chem.* **2004**, *76*, 1453.
[38] K. H. Lee, C. K. Chiang, Z. H. Lin, H. T. Chang, *Rapid Commun. Mass Spectrom.* **2007**, *21*, 2023.
[39] T. Watanabe, K. Okumura, H. Kawasaki, R. Arakawa, *J. Mass Spectrom.* **2009**, *44*, 1443.
[40] W. Y. Chen, Y. C. Chen, *Anal. Bioanal. Chem.* **2006**, *386*, 699.
[41] C. T. Chen, Y. C. Chen, *Anal. Chem.* **2005**, *77*, 5912.
[42] H. Kawasaki, T. Yonezawa, T. Watanabe, R. Arakawa, *J. Phys. Chem. C* **2007**, *111*, 16278.
[43] J. A. McLean, A. A. Stumpo, D. H. Russell, *J. Am. Chem. Soc.* **2005**, *127*, 5304.
[44] Y. F. Huang, H. T. Chang, *Anal. Chem.* **2006**, *78*, 1485.
[45] H. P. Wu, C. L. Su, H. C. Chang, W. L. Tseng, *Anal. Chem.* **2007**, *79*, 6215.
[46] E. T. Castellana, D. H. Russell, *Nano Lett.* **2007**, *7*, 3023.
[47] K. Shibamoto, K. Sakata, K. Nagoshi, T. Korenaga, *J. Phys. Chem. C* **2009**, *113*, 17774.
[48] S. D. Sherrod, A. J. Diaz, W. K. Russel, P. S. Cremer, D. H. Russell, *Anal. Chem.* **2008**, *80*, 6796.
[49] T. C. Chiu, L. C. Chang, C. K. Chiang, H. T. Chang, *J. Am. Soc. Mass Spectrom.* **2009**, *20*, 2008.
[50] H. Kawasaki, T. Akira, T. Watanabe, K. Nozaki, T. Yonezawa, R. Arakawa, *Anal. Bioanal. Chem.* **2009**, *395*, 1423.
[51] S. K. Kailasa, K. Kiran, H. F. Wu, *Anal. Chem.* **2008**, *80*, 9681.
[52] K. Shrivas, S. K. Kailasa, H. F. Wu, *Proteomics* **2009**, *9*, 2656.
[53] Z. Chen, Z. Geng, D. Shao, Y. Mei, Z. Wang, *Anal. Chem.* **2009**, *81*, 7625.
[54] S. Alimpiev, S. Nikiforv, V. Karavanskii, T. Minton, J. Sunner, *J. Chem. Phys.* **2001**, *115*, 1891.
[55] R. A. Kruse, X. Li, P. W. Bohn, J. V. Sweedler, *Anal. Chem.* **2002**, *74*, 3639.

  

[56] Y. Chen, H. Chen, A. Aleksandrov, T. M. Orlando, *J. Phys. Chem. C* **2008**, *112*, 6953.
[57] S. A. Trauger, E. P. Go, Z. Shen, J. V. Apon, B. J. Compton, E. S. P. Bouvier, M. G. Finn, G. Siuzdak, *Anal. Chem.* **2004**, *76*, 4484.
[58] G. Luo, Y. Chen, G. Siuzdak, A. Vertes, *J. Phys. Chem. B* **2005**, *109*, 24450.
[59] S. Dagan, Y. Hua, D. J. Boday, A. Somogyi, R. J. Wysocki, V. H. Wyoski, *Int. J. Mass. Spectrom.* **2009**, *283*, 200.
[60] T. R. Northen, H. K. Woo, M. T. Northen, A. Nordström, W. Uritboonthai, K. L. Turner, G. Siuzdak, *J. Am. Soc. Mass Spectrom.* **2007**, *18*, 1945.
[61] Y. Wada, T. Yanagishita, H. Masuda, *Anal. Chem.* **2007**, *79*, 9122.
[62] H. W. Tang, K. M. Ng, W. Lu, C. M. Che, *Anal. Chem.* **2009**, *81*, 4720.
[63] T. Yonezawa, H. Kawasaki, A. Tarui, T. Watanabe, R. Arakawa, T. Shimada, F. Mafune, *Anal. Sci.* **2009**, *25*, 339.
[64] W. Y. Chen, L. S. Wang, H. T. Chiu, Y. C. Chen, *J. Am. Soc. Mass Spectrom.* **2004**, *15*, 1629.
[65] Q. Liu, Y. Xiao, C. Pagan-Miranda, Y. M. Chiu, L. He, *J. Am. Soc. Mass Spectrom.* **2009**, *20*, 80.
[66] I. Lombardi, S. Marchinna, G. Zangaru, S. Pizzini, *Langmuir* **2007**, *23*, 12413.
[67] M. Cerruti, G. Doerk, G. Hernandez, C. Carraro, R. Maboudian, *Langmuir* **2010**, *26*, 432.
[68] T. Yao, H. Kawasaki, T. Watanabe, R. Arakawa, *Int. J. Mass Spectrom.* **2010**, *291*, 145.
[69] R. F. Sekerka, *Cryst. Res. Technol.* **2005**, *40*, 291.
[70] K.-S. Choi, *Dalton Trans.* **2008**, *40*, 5389.
[71] M. Sadeghi, W. Liu, T. G. Zhang, P. Stavropoulos, B. Levy, *J. Phys. Chem.* **1996**, *100*, 19466.
[72] S. Sakthivel, M. V. Shankar, M. Palanichamy, B. Arabindoo, D. W. Bahnemann, V. Murugesan, *Water Res.* **2004**, *38*, 3001.
[73] G. Luo, I. Marginean, A. Vertes, *Anal. Chem.* **2002**, *74*, 6185.
[74] G. Luo, Y. Chen, H. Daniels, R. Dubrow, A. Vertes, *J. Phys. Chem. B* **2006**, *110*, 13381.
[75] L. P. Law, *Int. J. Mass Spectrom.* **2010**, *290*, 72.
[76] N. Tian, Z. Y. Zhou, Z. G. Sun, L. Cui, B. Ren, Z. Q. Tian, *Chem. Commun.* **2006**, 4090.
[77] M. Subhramannia, V. K. Pillai, *J. Mater. Chem.* **2008**, *18*, 5858.
[78] J. N. Tiwari, F. M. Pan, K. L. Linb, *New J. Chem.* **2009**, *33*, 1482.

Received: April 21, 2010
Published online: August 2, 2010

  